Biomaterials Science

ROYAL SOCIETY OF CHEMISTRY

PAPER

View Article Online
View Journal | View Issue

Cite this: *Biomater. Sci.*, 2024, **12**, 1707

A highly tuneable inverse emulsion polymerization for the synthesis of stimuli-responsive nanoparticles for biomedical applications

Andrew C. Murphy,†[a,b] Heidi F. Oldenkamp†[a,b] and Nicholas A. Peppas *[a,b,c,d,e]

Polymeric nanomaterials have seen widespread use in biomedical applications as they are highly tuneable to achieve the desired stimuli-responsiveness, targeting, biocompatibility, and degradation needed for fields such as drug delivery and biosensing. However, adjustments to composition and the introduction of new monomers often necessitate reoptimization of the polymer synthesis to achieve the target parameters. In this study, we explored the use of inverse emulsion polymerization to prepare a library of polymeric nanoparticles with variations in pH and temperature response and examined the impact of overall batch volume and the volume of the aqueous phase on nanoparticle size and composition. We were able to prepare copolymeric nanoparticles using three different nonionic and three different anionic comonomers. Varying the non-ionizable comonomers, acrylamide (AAm), 2-hydroxyethyl methacrylate, and *N*-isopropylacrylamide (NIPAM), was found to alter the mass percentage of methacrylic acid (MAA) incorporated (from 26.7 ± 3.5 to 45.8 ± 1.8 mass%), the critical swelling pH (from 5.687 ± 0.194 to 6.637 ± 0.318), and the volume swelling ratio (from 1.389 ± 0.064 to 2.148 ± 0.037). Additionally, the use of NIPAM was found to allow for temperature-responsive behavior. Varying the ionizable comonomers, MAA, itaconic acid, and 2-acrylamido-2-methylpropane sulfonic acid (AMPSA), was found to significantly alter the critical swelling pH and, in the case of AMPSA, remove the pH-responsive behavior entirely. Finally, we found that for the base P(AAm-*co*-MAA) formulation, the pH-responsive swelling behavior was independent of the scale of the reaction; however, variations in the aqueous volume relative to the volume of the continuous phase significantly affected both the nanoparticle size and the critical swelling pH.

Received 30th October 2023,
Accepted 6th February 2024

DOI: 10.1039/d3bm01765f

rsc.li/biomaterials-science

Introduction

Polymer nanoparticles are an important class of materials with wide-ranging applications in biomedicine. Applications include drug delivery, regenerative medicine, and biosensing.[1–5] Hydrogel nanoparticles, or nanogels, are especially desirable due to their highly tuneable properties such as size, chemical composition, surface functionality, and environmental responsiveness.[6] For the controlled release of drugs, the drug cargo can be loaded into or onto the particle in various ways, such as entrapment, encapsulation, or attachment.[7] Specifically, nanoparticles with a diameter less than 200 nm are desirable due to the enhanced permeation and retention (EPR) effect, which is especially relevant in drug delivery for cancer treatment due to the increased particle residence time in solid tumors, which can be attributed to their unique vasculature.[8] These nanoparticles can be surface-modified, such as with PEG grafts, to camouflage them and avoid rapid clearance by the mononuclear phagocytic system after injection into the body.[9] Applications in regenerative medicine include the fabrication of nanocomposite hydrogels, in which polymeric nanoparticles can be embedded within a bulk matrix or scaffold, such as a natural hydrogel, for the delivery of agents such as growth factors in tissue engineering.[10] In the field of biosensing, polymeric nanoparticles can be incorporated into devices which show potential for the detection of a wide variety of molecules, which could contribute to disease diagnosis, environmental monitoring, and improved food safety.[11]

One common method used to synthesize uniform nanogels is emulsion polymerization, in which hydrophobic monomer droplets are suspended in a continuous aqueous phase and stabilized by surfactant(s).[12–15] This method is useful for the

[a]*McKetta Department of Chemical Engineering, The University of Texas at Austin, Austin, TX, 78712, USA. E-mail: peppas@che.utexas.edu*
[b]*Institute for Biomaterials, Drug Delivery, and Regenerative Medicine, The University of Texas at Austin, Austin, TX, 78712, USA*
[c]*Department of Biomedical Engineering, The University of Texas at Austin, Austin, TX, 78712, USA*
[d]*Department of Surgery and Perioperative Care, Dell Medical School, The University of Texas at Austin, Austin, TX, 78712, USA*
[e]*Division of Pharmaceutics, College of Pharmacy, The University of Texas at Austin, Austin, TX, 78712, USA*
†These authors contributed equally.

encapsulation of hydrophobic cargos but presents a challenge if it is desired to load a hydrophilic compound due to partitioning of the nanogels in the organic phase.[16] As shown in Fig. 1, inverse emulsion polymerization utilizes a water-in-oil approach in which the water-soluble monomers and crosslinker are dissolved in the aqueous phase and then suspended in a continuous organic phase and stabilized by surfactants to form a nanoemulsion.[17–19] This technique is useful for the encapsulation of hydrophilic compounds such as proteins.[20–23] It has also been demonstrated that it is possible to incorporate environmentally-responsive crosslinkers within inverse emulsion-synthesized nanogels, which allows them to degrade under desired conditions to release a payload.[20–22] Recent work in our lab explored the inverse emulsion polymerization of poly(acrylamide-*co*-methacrylic acid) (P(AAm-*co*-MAA)) nanogels and found the method to be a robust strategy for the preparation of pH-responsive nanoparticles for biomedical applications with the ability to reproducibly tune the size of the nanoparticles through manipulation of the reaction conditions.[24] However, additional questions remain regarding the scalability of the polymerization, the degree to which nanoparticle composition is influenced by reaction conditions, and the accessibility of inverse emulsion polymerization to other biomedically-relevant polymers.

We hypothesized that the inverse emulsion polymerization technique used to synthesize tuneable P(AAm-*co*-MAA) nanoparticles demonstrated in Zhong *et al.* could be translated to other water-soluble comonomers without compromising the micelle stability and resulting nanoparticles. Specifically, we were interested in changing the identity of the non-ionizable and ionizable monomers (*i.e.* change acrylamide (AAm) to *N*-isopropyl acrylamide (NIPAM) or 2-hydroxyethyl methacrylate (HEMA) or swap methacrylic acid (MAA) for itaconic acid (IA) or 2-acrylamido-2-methylpropane sulfonic acid (AMPSA)). By changing the monomers used, we hypothesized that not only the hydrodynamic diameter, but also the pH- and temperature-responsive behavior could be altered within a single synthetic platform.

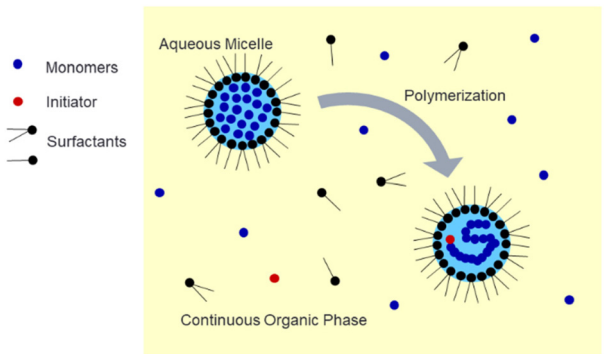

Fig. 1 Inverse emulsion polymerization scheme depicting water-soluble comonomers and crosslinker dissolved in the aqueous phase and stabilized by surfactants in the continuous organic phase. Figure adapted with permission from Zhong *et al.*

Additionally, we wanted to determine the effect of changing the overall batch size or aqueous phase volume used during particle synthesis on the chemical composition and pH-responsive behavior of the P(AAm-*co*-MAA) nanoparticles. Zhong *et al.* evaluated the impact of many polymerization parameters on the composition and behavior of the P(AAm-*co*-MAA) nanogels, including but not limited to comonomer ratio, total monomer concentration, crosslinking density, and surfactant concentration, but the effect of the batch size and aqueous phase volume were not evaluated. We were interested in exploring whether this platform could be scaled to varying batch sizes without negatively impacting the nanogel properties, which could potentially be useful for scale-up to industrial production. We believe that inverse emulsion polymerization is a useful synthesis technique that can be used to create a wide range of particles for varying biomedical applications.

Experimental

Materials and methods

Materials, instrumentation, and analysis. All reagents were purchased from Fisher Scientific, Sigma Aldrich, or Argos Organics and used as received. A Thermo Scientific Barnstead GenPure purification system (18.2 MΩ) was used to obtain ultrapure water. Potentiometric titrations of nanoparticle suspensions were performed using a Hanna Instruments HI 902 potentiometric titrator. Fourier-Transform Infrared (FTIR) spectra were collected using a Thermo Scientific Nicolet is10 FT-IR spectrometer. Dynamic light scattering and zeta potential measurements were obtained with a Malvern ZetaSizer Nano-ZS equipped with a He–Ne 633 nm laser in a back-scattering arrangement and attached MPT-2 Multi-Purpose Titrator accessory. Statistical analysis was performed using Graphpad Prism.

Nanoparticle synthesis. Hydrogel nanoparticles were prepared by inverse emulsion free-radical polymerization using a method adapted from Zhong *et al.*[24] Briefly, comonomers (combined concentration 4.868 M, 3 : 1 molar feed ratio of non-ionizable comonomer to ionizable comonomer for all formulations) and methylenebisacrylamide crosslinker (202.8 mM) were dissolved in ultrapure water along with *N*,*N*,*N*′,*N*′-tetramethylethylenediamine. Exact volumes used are listed in Table 1. The aqueous solution was placed in a bath sonicator for 10 minutes to ensure complete dissolution of all compounds and homogeneity. To comprise the organic phase, surfactants Brij-30 (151.4 mM) and dioctyl sulfosuccinate (AOT, 30.3 mM) were added to hexanes and stirred in a round bottom flask at 500 rpm until dissolved. For the P(AAm-*co*-IA) formulations, a 10 : 1 ratio of surfactants (Brij-30 to AOT) was used due to increased particle stability with a higher ratio of non-ionic to ionic surfactant, but the total concentration of surfactants remained the same (total surfactant concentration 181.7 mM, 165.2 mM Brij-30 and 16.5 mM AOT).

A specified volume of the aqueous phase was then added to the organic phase to form the pre-polymer emulsion. The

Table 1 Variables chosen for each formulation of nanoparticles synthesized *via* inverse emulsion polymerization. Variables include the non-ionizable comonomer and ionizable comonomer identities and the aqueous and organic phase volumes. Other considerations, such as round bottom flask volume, TEMED volume, and APS volume, were scaled according to the organic phase volume

Non-ionizable comonomer	Ionizable comonomer	Aqueous phase volume (mL)	Organic phase hexanes volume (mL)	Round bottom flask volume (mL)	TEMED volume (μL)	APS volume (μL)
AAm	MAA	0.875	30	100	12.5	37.5
AAm	MAA	1.75	30	100	25	75
AAm	MAA	3.5	30	100	50	150
AAm	MAA	0.4375	7.5	25	6.25	18.75
AAm	MAA	3.5	60	200	50	150
AAm	IA	1.75	30	100	25	75
AAm	AMPSA	1.75	30	100	25	75
NIPAM	MAA	1.75	30	100	25	75
HEMA	MAA	1.75	30	100	25	75

emulsion was purged with nitrogen gas for 20 minutes at 215 mL per minute to remove free radical scavengers. Then, a specified volume of initiator solution (100 mg mL^{-1} ammonium persulfate in ultrapure water) was added to the pre-polymer emulsion flask and it was purged with nitrogen for an additional 10 minutes. Reactions were allowed to polymerize overnight (or for 72 hours for P(AAm-*co*-IA) formulations) under constant stirring (500 rpm) at room temperature.

Nanoparticle purification. At the indicated endpoint, the P(AAm-*co*-MAA), P(AAm-*co*-IA), and P(AAm-*co*-AMPSA) nanoparticles were purified by mixing with an equivalent volume of ethanol and centrifuge at 3200*g* for five minutes. The nanoparticles were resuspended in ethanol, and the process was repeated three times. The nanoparticles were then dialyzed against a water/ethanol gradient of 1 : 1 (2 changes), 3 : 1 (2 changes), 7 : 1 (1 change), 15 : 1 (1 change), ultrapure water (4 changes). Dialysis for the P(AAm-*co*-IA) formulation began with a 1 : 3 ratio of water to ethanol and then proceeded as described.

P(NIPAM-*co*-MAA) and P(HEMA-*co*-MAA) nanoparticles were mixed with an equivalent volume of tetrahydrofuran and centrifuged at 3200*g* for ten minutes one time. The nanoparticles were resuspended in a 50 : 50 vol% ethanol/water mixture and immediately dialyzed against the same water/ethanol gradient as P(AAm-*co*-MAA). Following dialysis, a portion of the nanoparticle suspension was lyophilized to determine the particle concentration (mg mL^{-1}) and for further characterization.

Potentiometric titration. For each formulation, the nanoparticles were suspended in 5 mM potassium chloride at 0.167 mg mL^{-1} (10 mg of nanoparticles in 60 mL of 5 mM potassium chloride). The pH was raised above 10 with 1 N sodium hydroxide and then titrated down to pH 3.0 with 0.01 N hydrochloric acid. The results were compared to a blank of 5 mM potassium chloride alone that was similarly titrated. The pK_a and acid content were determined by finding the largest derivative of the curve at the shoulder for the MAA and then subtracting the moles of acid required to titrate the blank to the same pH. The resulting number of moles was equivalent to half the number of moles of MAA in the nanoparticles as only half of the MAA groups will be protonated when the pH is equal to the pK_a.

Fourier-transform infrared spectroscopy (FTIR). Following dialysis, portions of the nanoparticle suspensions were lyophilized to obtain a dry particle powder, which was used to collect FTIR spectra from 4000 to 600 cm^{-1} and the background absorbance was subtracted. Absorbance spectra are presented as the average of 64 scans and were normalized to the maximum absorbance value.

Dynamic light scattering. All formulations were subjected to autotitration to assess the pH-responsive swelling behavior. Nanoparticle formulations were diluted to 0.5 mg mL^{-1} in 1× PBS and introduced to the titration accessory, which circulates the sample to the ZetaSizer for DLS analysis. The autotitrator enables constant stirring of the sample and had the ability to draw from three titrants: 1 N HCl, 0.1 N HCl, and 0.1 N NaOH. All samples were initially adjusted to pH 9 ± 0.1 and the titrator gradually decreased the pH until a final pH of 3 was reached. From pH 9 to 7, size measurements were taken at increments of 0.3 pH units. From pH 7 to 5, an increment of 0.2 was used in order to more completely capture the swelling transition of the formulations. From pH 5 to 3, size measurements were taken at intervals of 0.5 pH units. Once a pH of 3 was reached, the titrator returned the sample to pH 9 using the same increments as when titrating from high to low pH. For all samples, three independent size measurements were collected at each pH increment and three identical batches were tested for each formulation. The curves were then fit to a nonlinear equation of the form shown in eqn (1) and values for A, B, C, and D were determined. In this equation, A is the collapsed diameter of the particles, B is the slope of the swelling transition, C is the critical swelling pH, and D is the swollen diameter of the particles. The constants were averaged across the triplicates and the resulting equation was used to plot the average swelling profile for each formulation. In cases where aggregation was observed at lower pH, those points were omitted from the logistical curve fit.

$$D_h = \frac{A - D}{1 + \exp[B(\mathrm{pH} - C)]} + D \quad (1)$$

Select nanoparticle formulations (P(AAm-*co*-MAA) and P(NIPAM-*co*-MAA)) were also subject to DLS measurements

over a range of temperatures to observe the effect of temperature on particle swelling behavior. For these experiments, the nanoparticles were diluted to 0.5 mg mL^{-1} in 1× PBS and adjusted to pH 7.4. The sample was placed in a quartz cuvette inside the ZetaSizer and the temperature of the sample was increased from 19 to 55 °C in increments of 3 °C and the nanoparticle size was measured at each step.

Zeta potential measurements were collected using folded capillary zeta cells. The nanoparticle formulations were diluted to 2 mg mL^{-1} in 5 mM sodium phosphate buffer and adjusted to pH 7.4. Measurements were taken in triplicate, with each measurement representing an average of >10 runs.

Results and discussion

Nanoparticle chemical composition

Potentiometric titration. The MAA content of the nanoparticles as determined by potentiometric titration is shown in Table 2. Comparing the impact of changing the batch size on MAA content for the P(AAm-*co*-MAA) formulations, the mass percent of MAA was found to be comparable across all batch sizes. When examining the effect of changing the aqueous volume of the emulsion, the MAA mass percent was found to increase with increasing volume, which may be explained by differences in the ability of MAA to partition into the hexanes, although the difference was not significant. For the potentiometric titration curves of the three different non-ionizable, hydrophilic comonomers shown in Fig. 2A, there were significant differences observed in the mass percent of MAA between P(AAm-*co*-MAA) and both P(HEMA-*co*-MAA) and P(NIPAM-*co*-MAA) as determined by one-way ANOVA ($p < 0.0001$); however, the differences in mass percent of the three formulations trended with the molecular weight of their respective comonomers (HEMA 130.14 g mol^{-1}, NIPAM 113.16 g mol^{-1}, AAm 71.08 g mol^{-1}) and were not found to be significant when compared to the initial mass percent of the feed. In all cases the final mass% of MAA in the nanoparticles exceeded the amount in the monomer feed. One possibility for the increased MAA content could be the hydrolysis of the amides and esters in the hydrophilic comonomers as reported previously;[24] however, the avoidance of strong acid or bases during the purification process was expected to limit the rate at which hydrolysis occurs. Another potential possibility is preferential incorporation of methacrylic acid over the respective non-ionizable comonomer (AAm, NIPAM, or HEMA).

Table 2 Calculated MAA content of the nanoparticle formulations based on potentiometric titrations

Formulation name (volume aqueous phase (mL)/volume hexanes in organic phase (mL))	Measured MAA mass% (mean ± SD)	Ratio of measured MAA mass% to feed MAA mass % (mean ± SD)
P(AAm-*co*-MAA) 0.875/30	41.0 ± 4.2	1.548 ± 0.158
P(AAm-*co*-MAA) 1.75/30	45.8 ± 1.2	1.730 ± 0.046
P(AAm-*co*-MAA) 3.5/30	50.3 ± 5.7	1.899 ± 0.215
P(AAm-*co*-MAA) 0.4375/7.5	45.5 ± 2.5	1.717 ± 0.093
P(AAm-*co*-MAA) 3.5/60	46.0 ± 1.7	1.737 ± 0.066
P(NIPAM-*co*-MAA) 1.75/30	31.6 ± 1.1	1.656 ± 0.056
P(HEMA-*co*-MAA) 1.75/30	26.7 ± 3.5	1.560 ± 0.202

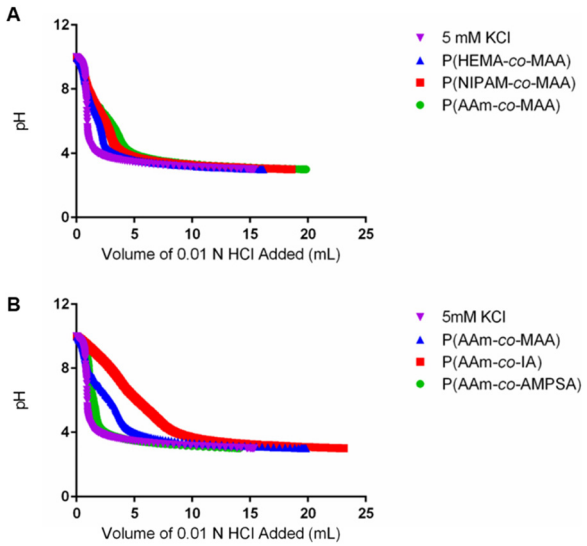

Fig. 2 Potentiometric titration curves of representative samples of the formulations with varying (A) non-ionizable hydrophilic and (B) ionizable comonomers.

As shown in Fig. 2B, more apparent differences were observed in the buffering capacity of the formulations with different ionizable comonomers in comparison to those with different non-ionizable comonomers. P(AAm-*co*-AMPSA) showed little deviation from 5 mM potassium chloride while P(AAm-*co*-IA) had more acid content than P(AAm-*co*-MAA) and thus required a larger volume of titrant to overcome its buffering capacity; however, neither formulation displayed a prominent shoulder that could be used to determine pK_a and acid content. In the case of P(AAm-*co*-AMPSA), the sulfonic acid likely remained ionized at pH 3 so no shoulder was observed over the measured range. As IA has two ionizable groups per unit with similar pK_a values, the protonation of the two groups overlapped and obscured the individual transitions. As a result, it was not possible to calculate precise acid content for P(AAm-*co*-IA) using the same method as was used for MAA, but the greater HCl volume needed for the titration compared to P(AAm-*co*-MAA) is indicative of a greater total acid content.

FTIR. Using FTIR, the expected chemical composition of the nanoparticle formulations was confirmed. Spectra of each of the formulations synthesized using 1.75 mL aqueous phase and 30 mL hexanes in the organic phase are shown in Fig. 3. Only the region from 1800–600 cm^{-1} is shown because there were no noteworthy differences in the spectra from 4000–1800 cm^{-1}. For the P(AAm-*co*-MAA) formulation, the spectrum closely matches that described by Zhong *et al.* when purified using the same method described here (precipitation

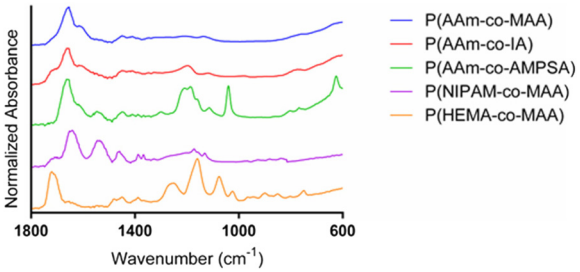

Fig. 3 FTIR spectra obtained from polymer nanoparticles synthesized using inverse emulsion polymerization and normalized to each spectrum's largest peak. Characteristic peaks confirm the expected chemical composition.

in ethanol and dialysis against a water : ethanol gradient). The most prominent peak is found at 1654 cm^{-1}, which is indicative of the stretching of the acrylamide carbonyl groups. The shoulder around 1610 cm^{-1} and smaller peak at 1440 cm^{-1} is indicative of carbonyl stretching in deprotonated carboxylates. The spectrum for P(AAm-*co*-IA) is similar to that of P(AAm-*co*-MAA), with the main differences being the addition of a shoulder on the carbonyl peak around 1710 cm^{-1} (which can be attributed to the increased presence of carboxylic acid groups in comparison to MAA) and a small peak at 1190 cm^{-1} (C–O). The strong acrylamide peak demonstrated in P(AAm-*co*-MAA) and carboxylate anion peaks are also present in the spectra for P(AAm-*co*-IA). P(AAm-*co*-AMPSA) nanoparticles also resulted in a spectrum with a strong acrylamide peak around 1663 cm^{-1}. The peak at 1040 cm^{-1} and collection of peaks from 1140–1240 cm^{-1} are indicative of the sulfonic acid group on AMPSA. The peak at 625 cm^{-1} can be attributed to S-OR species. For the P(NIPAM-*co*-MAA) formulation, we observed a peak at 1705 cm^{-1}, which is indicative of the carboxylic acid group on MAA and a series of 3 successively smaller peaks at 1635, 1530, and 1455 cm^{-1}, which are characteristic of NIPAM. Finally, for P(HEMA-*co*-MAA), we observed a strong C═O peak around 1710 cm^{-1} and C–O–C peaks indicative of HEMA between 1300–1000 cm^{-1}. There were no differences in the FTIR spectra for identical batches (synthesized in triplicate) and all synthesized formulations of P(AAm-*co*-MAA) resulted in identical FTIR spectra despite the differing aqueous phase and overall batch volumes.

Stimuli-responsive swelling behavior of the nanoparticles

Impact of comonomer on pH-dependent and temperature-responsive swelling behavior. The average swelling profile for each of the different comonomer formulations is shown in Fig. 4. These curves were then used to calculate the volume swelling ratios for the formulations, which are shown in Fig. 5. Looking first at the impact of the choice of non-ionizable hydrophilic comonomer, P(AAm-*co*-MAA) showed the greatest volume swelling ratio followed by P(NIPAM-*co*-MAA) and then P(HEMA-*co*-MAA), although these differences were not significant and trended with the hydrodynamic diameter of the swollen nanoparticle (Fig. 4A), which was largest for P(AAm-*co*-

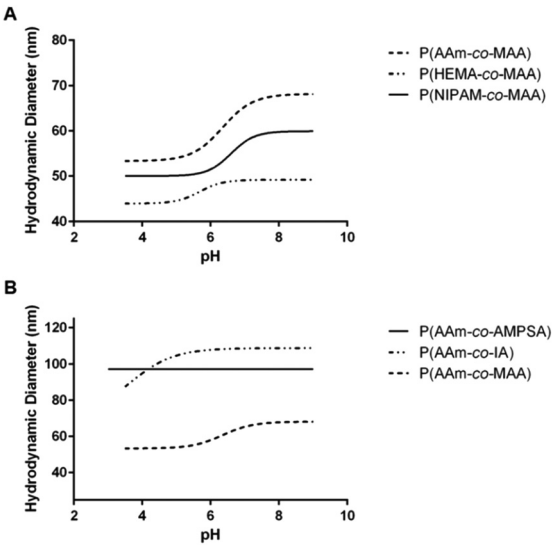

Fig. 4 Average swelling profile for each of the different comonomer formulations of (A) non-ionizable hydrophilic and (B) ionizable comonomers.

MAA). In the case of both P(HEMA-*co*-MAA) and P(NIPAM-*co*-MAA), aggregation was observed as the pH approached the pK_a of MAA that led to an increase in the measured hydrodynamic diameter, and these points were omitted from the fit to the data. The critical swelling pH and maximum volume swelling ratio are reported in Table 3. For these three formulations, the critical swelling pH ranged from 5.69 ± 0.19 for P(HEMA-*co*-MAA) to 6.64 ± 0.32 for P(NIPAM-*co*-MAA), but these values were not significantly different as determined by one-way ANOVA.

Comparing the effect of different ionizable comonomers (Fig. 4B), P(AAm-*co*-AMPSA) most notably did not show any swelling or collapse over the tested pH range, which was due to the sulfonic acid remaining fully ionized over the measured range, and so it was excluded from further analysis. Similar to P(NIPAM-*co*-MAA) and P(HEMA-*co*-MAA), P(AAm-*co*-IA) exhibited aggregation as it approached the pK_a values of the carboxylic acid groups in IA; however, unlike the other formulations, the aggregation occurred before the nanoparticles had reached their fully collapsed diameter.

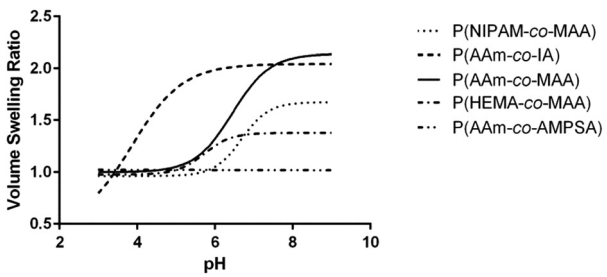

Fig. 5 Volume swelling ratio as a function of pH for all comonomer formulations.

Table 3 Critical swelling pH and maximum volume swelling ratio for all formulations with varying comonomer composition determined using logistic fit curves

Formulation	Critical swelling pH (mean ± SEM)	Maximum volume swelling ratio (mean ± SD)
P(AAm-*co*-MAA)	6.329 ± 0.058	2.148 ± 0.037
P(NIPAM-*co*-MAA)	6.637 ± 0.318	1.693 ± 0.378
P(HEMA-*co*-MAA)	5.678 ± 0.194	1.389 ± 0.064
P(AAm-*co*-IA)	3.604 ± 0.597	2.068 ± 0.444
P(AAm-*co*-AMPSA)	N/A	1.048 ± 0.008

For the purposes of comparison, the smallest hydrodynamic diameter of the nanoparticles prior to aggregation was used to calculate the volume swelling ratio, although this resulted in the collapsed volume swelling ratio predicted from the data fit to be below 1. For the determined volume swelling ratio at the fully swollen condition, P(AAm-*co*-IA) had the second greatest volume swelling ratio, although this was found to not be significantly different from any of the other formulations. P(AAm-*co*-IA) also had the largest swollen hydrodynamic diameter of the tested comonomer formulations. However, P(AAm-*co*-IA) was found to have a significantly lower critical swelling pH than P(AAm-*co*-MAA), P(NIPAM-*co*-MAA), and P(HEMA-*co*-MAA) as determined by one-way ANOVA. One possible explanation for this is that the greater density of carboxylic acid groups and broader pH range over which protonation occurs increased electrostatic repulsion and enabled the P(AAm-*co*-MAA) nanoparticles to remain swollen until lower pH values than those with MAA. From these findings, altering the choice of comonomer can be used to adjust the stability and critical swelling pH of the nanoparticles to suit the demands of a particular application.

Additionally, NIPAM has been studied for its ability to form temperature-responsive polymers, which have many applications in drug delivery and regenerative medicine. In order to examine the impact of inverse emulsion polymerization on the temperature responsiveness of P(NIPAM-*co*-MAA) nanoparticles, the hydrodynamic diameter as a function of temperature was measured for P(NIPAM-*co*-MAA) and P(AAm-*co*-MAA) nanoparticles (Fig. 6). Across the measured temperature range, P(NIPAM-*co*-MAA) exhibits a significant decrease in hydrodynamic diameter ($p = 0.033$), which is not observed in P(AAm-*co*-MAA). This data confirms that the inverse emulsion polymerization does not negatively affect the temperature-responsive properties of the nanogels containing NIPAM.

Impact of overall batch volume on pH-dependent swelling behavior. The overall batch volume while synthesizing P(AAm-*co*-MAA) nanoparticles had little impact on the nanoparticle diameter and swelling behavior. As shown in Fig. 7A, the hydrodynamic diameter of the nanoparticles ranged from approximately 55 nm in the collapsed state to 65–70 nm in the swollen state for all three variations in batch size that were measured (0.4375 mL/7.5 mL, 1.75 mL/30 mL, and 3.5 mL/60 mL). When fit to a logistic curve, the critical swelling pH of each formulation could be determined and these values are shown in Table 4. As determined with a one-way ANOVA and Tukey's multiple comparisons test, there was no significant difference in critical swelling pH between the three batch sizes that were evaluated. When the volume swelling ratio of these formulations was calculated, there was even less of a difference in the logistical fit curves as a function of pH (Fig. 7B). There was also no significant difference in the maximum volume swelling ratio for each of these three formulations. This demonstrates that this synthesis scheme could easily be scaled up for larger scale manufacturing purposes without significantly changing the swelling behavior of the particles.

Impact of aqueous phase volume on pH-dependent swelling behavior. When the aqueous phase volume was varied (0.875 mL, 1.75 mL, and 3.5 mL) while keeping the volume of hexanes in the organic phase constant (30 mL), more variation

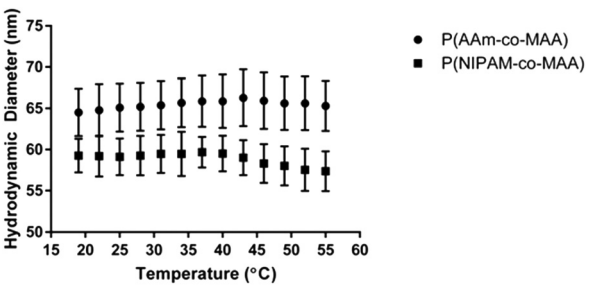

Fig. 6 Temperature swelling curve of P(AAm-*co*-MAA) and P(NIPAM-*co*-MAA) nanoparticle formulations.

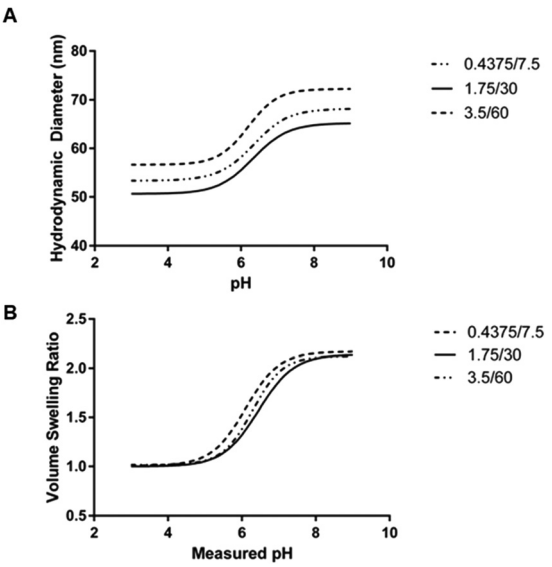

Fig. 7 Average logistic regression curves for P(AAm-*co*-MAA) nanoparticle swelling behavior plotted as (A) hydrodynamic diameter and (B) volume swelling ratio as a function of pH when changing the overall batch volume used for synthesis. Each curve is the logistic regression fit of 3–4 independent swelling curves for each formulation. Values in the legend are reported as "aqueous phase volume/organic phase hexanes volume" (both in mL).

Table 4 Critical swelling pH and maximum volume swelling ratio for P(AAm-*co*-MAA) nanoparticles synthesized with varying overall batch sizes (n = 3–4 for each formulation, no significant differences in either parameter between formulations)

Aqueous phase volume (mL)	Organic phase hexanes volume (mL)	Critical swelling pH (mean ± SEM)	Maximum volume swelling ratio (mean ± SD)
0.4375	7.5	6.353 ± 0.080	2.182 ± 0.217
1.75	30	6.329 ± 0.058	2.148 ± 0.037
3.5	60	6.189 ± 0.086	2.140 ± 0.032

in the swelling behavior of the particles were observed. The formulations synthesized with the smallest aqueous phase volume swelled from a hydrodynamic diameter of approximately 35 nm at pH 3 to 45 nm at pH 9. In comparison, the particles synthesized with 3.5 mL of aqueous phase had a hydrodynamic diameter of approximately 95 nm when collapsed and 115 nm in the swollen state. The diameter of the particles synthesized with an intermediate volume of aqueous phase (1.75 mL) fell between those formulations, as shown in Fig. 8A. The varying particle diameter can be attributed to the number of surfactant molecules available to form micelles in the nanoemulsion when the aqueous phase is added to the organic phase. When a smaller volume of aqueous phase is used in synthesis, there is a proportionally higher number of surfactant molecules that stabilize the aqueous droplets, causing the resulting polymer nanoparticles to be smaller. The inverse is true for the particles synthesized with 3.5 mL of aqueous phase. This increased volume while maintaining identical organic phase properties means that there are proportionally less surfactant molecules able to stabilize the aqueous phase droplets *via* micelle formation, which results in larger nanoparticles.

The mean critical swelling pH of the formulations synthesized with the smallest volume of aqueous phase solution was significantly lower than the other two aqueous phase volumes evaluated (as determined by a one-way ANOVA and Tukey's multiple comparisons test) and these values are shown in Table 5. Similarly to comparing the formulations synthesized with varying overall batch size, we plotted volume swelling ratio as a function of pH (Fig. 8B), which clearly shows the lower critical swelling pH for the formulation synthesized with the smallest aqueous phase volume. While this plot demonstrates a larger maximum volume swelling ratio for the intermediate aqueous phase volume, this difference was determined to not be statistically significant.

Table 5 Critical swelling pH and maximum volume swelling ratio for P(AAm-*co*-MAA) nanoparticles synthesized with varying aqueous phase volumes (n = 3 for each formulation)

Aqueous phase volume (mL)	Organic phase hexanes volume (mL)	Critical swelling pH (mean ± SEM)	Maximum volume swelling ratio (mean ± SD)
0.875	30	5.141 ± 0.201	1.932 ± 0.167
1.75	30	6.329 ± 0.058	2.148 ± 0.037
3.5	30	6.405 ± 0.112	1.926 ± 0.301

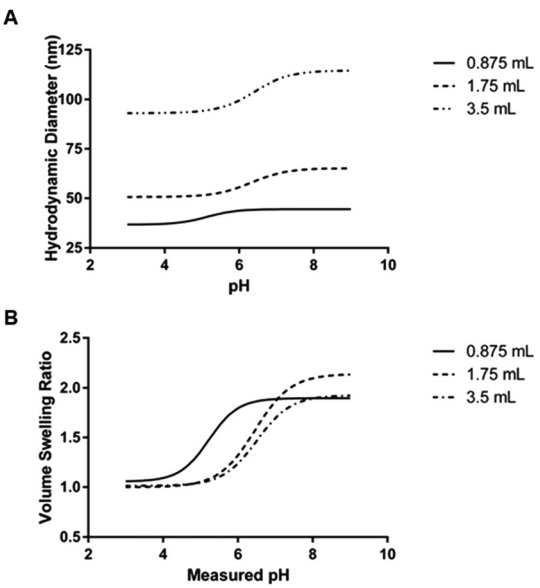

Fig. 8 Average logistic regression curves for P(AAm-*co*-MAA) nanoparticle swelling behavior plotted as (A) hydrodynamic diameter and (B) volume swelling ratio as a function of pH when changing the aqueous phase volume used for synthesis while keeping the organic phase volume constant (30 mL hexanes used for each formulation).

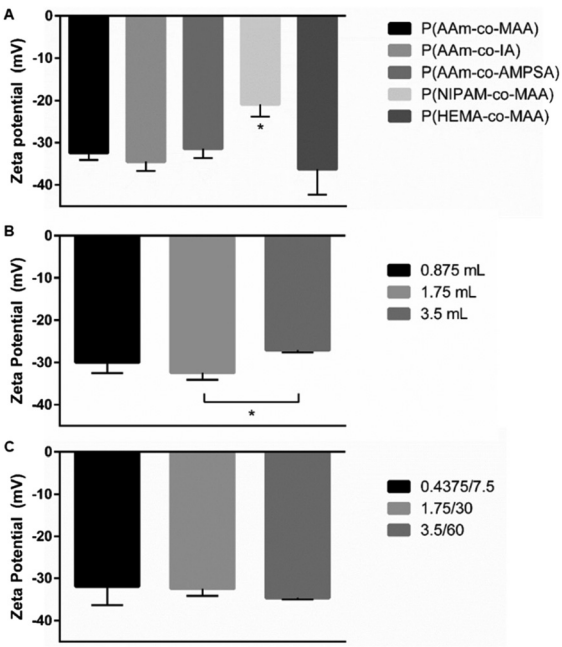

Fig. 9 Zeta potential measurements of the synthesized nanoparticle formulations at pH 7.4, varying monomer identity (A), P(AAm-*co*-MAA) aqueous phase volume (B), and P(AAm-*co*-MAA) overall batch size (C). Values in the legend are reported as "aqueous phase volume/organic phase hexanes volume", both in mL; data reported as mean ± SD, n = 3–6.

Impact of polymerization on polymer surface charge

The measured zeta potential for all formulations was negative, as expected for anionic polymer nanoparticles. For the five formulations when changing the non-ionic and ionic comonomer identity, shown in Fig. 9A, the P(NIPAM-*co*-MAA) particle zeta potential was statistically significant from all other formulations (significance determined with one-way ANOVA and Tukey's multiple comparisons test). When varying just the aqueous phase volume for P(AAm-*co*-MAA) syntheses (Fig. 9B), the difference in average zeta potentials for 1.75 mL and 3.5 mL aqueous phase volumes was statistically significant. This could be due to the larger particle diameter of the particles synthesized with 3.5 mL of aqueous phase. Larger particle diameter indicates larger surface area, which could reduce the density of MAA groups near the surface, leading to a slightly more neutral zeta potential. Finally, when scaling the entire batch size of the synthesized P(AAm-*co*-MAA) particles (Fig. 9C), there was no significant difference in average zeta potential between the three different formulations.

Conclusions

In this work, inverse emulsion polymerization was demonstrated as a synthesis platform for a wide range of polymeric nanomaterials. The batch size of the reaction was found to have negligible impact on several key parameters for biomedical applications, including volume swelling ratio, critical swelling pH, and MAA acid content, which suggests the system can be scaled to large batch sizes without negatively impacting the nanoparticles. Furthermore, the aqueous phase volume can be adjusted to tune the hydrodynamic diameter of the resulting nanoparticles. Finally, we demonstrated that this platform is extendable to a wide range of possible hydrophilic comonomers, both ionizable and non-ionizable, that can be used to impart new responsive behavior on the materials, such as variations in pH- and temperature-responsive compared to P(AAm-*co*-MAA) nanoparticles. The stimuli-responsive behavior of the synthesized nanoparticles could be desired in certain controlled drug delivery or regenerative medicine applications. While the results of this study focused on anionic comonomers only, future studies exploring the use of cationic comonomers would be valuable for applications such as biosensing or drug delivery of low pI biomacromolecules.

Author contributions

ACM and HFO contributed equally to the conceptualization, investigation, formal analysis, visualization, and writing – original draft. NAP was responsible for the resources, funding acquisition, supervision, and writing – review and editing.

Conflicts of interest

The authors declare no conflicts of interest.

Acknowledgements

The authors acknowledge financial support from the National Institutes of Health (R01-EB022025), the Cockrell Family Chair Foundation, and the office of the Dean of the Cockrell School of Engineering at the University of Texas at Austin for the Institute for Biomaterials, Drug Delivery, and Regenerative Medicine. ACM and HFO also acknowledge financial support from the National Science Foundation Graduate Research Fellowship Program (DGE-1610403). Any opinions, findings, and conclusions or recommendations expressed in this material are those of the author(s) and do not necessarily reflect the views of the funding agencies.

References

1 M. J. Mitchell, M. M. Billingsley, R. M. Haley, M. E. Wechsler, N. A. Peppas and R. Langer, *Nat. Rev. Drug Discovery*, 2020, **20**, 101–124.
2 L. Brannon-Peppas, *Int. J. Pharm.*, 1995, **116**, 1–9.
3 A. M. Wagner, M. P. Gran and N. A. Peppas, *Acta Pharm. Sin. B*, 2018, **8**, 147.
4 O. Z. Fisher and N. A. Peppas, *Macromolecules*, 2009, **42**, 3391–3398.
5 M. E. Wechsler, H. K. H. J. Dang, S. D. Dahlhauser, S. P. Simmonds, J. F. Reuther, J. M. Wyse, A. N. VandeWalle, E. V. Anslyn and N. A. Peppas, *Chem. Commun.*, 2020, **56**, 6141–6144.
6 A. Zielinska, F. Carreiró, A. M. Oliveira, A. Neves, B. Pires, D. N. Venkatesh, A. Durazzo, M. Lucarini, P. Eder, A. M. Silva, A. Santini and E. B. Souto, *Molecules*, 2020, **25**, 3731.
7 K. S. Soppimath, T. M. Aminabhavi, A. R. Kulkarni and W. E. Rudzinski, *J. Controlled Release*, 2001, **70**, 1–20.
8 E. Blanco, H. Shen and M. Ferrari, *Nat. Biotechnol.*, 2015, **33**, 941.
9 D. E. Owens and N. A. Peppas, *Int. J. Pharm.*, 2006, **307**, 93–102.
10 K. S. Suresh, S. Bhat, B. R. Guru, M. S. Muttigi and R. N. Seetharam, *Stem Cell Res. Ther.*, 2020, **11**, 1–14.
11 A. T. Silva, R. Figueiredo, M. Azenha, P. A. S. Jorge, C. M. Pereira and J. A. Ribeiro, *ACS Sens.*, 2023, **8**, 2898–2920.
12 K. Landfester, *Angew. Chem., Int. Ed.*, 2009, **48**, 4488–4507.
13 R. Muñoz-Espí and O. Álvarez-Bermúdez, *in Nanoemulsions: Formulation, Applications, and Characterization*, Academic Press, 2018, pp. 477–515.
14 A. S. Puranik, L. P. Pao, V. M. White and N. A. Peppas, *Eur. J. Pharm. Biopharm.*, 2016, **108**, 196–213.
15 A. Elzayat, I. Adam-Cervera, O. Álvarez-Bermúdez and R. Muñoz-Espí, *Colloids Surf., B*, 2021, **203**, 111764.
16 V. Daniloska, P. Carretero, R. Tomovska, M. Paulis and J. M. Asua, *ACS Appl. Mater. Interfaces*, 2014, **6**, 3559–3567.
17 M. Antonietti and K. Landfester, *Prog. Polym. Sci.*, 2002, **27**, 689–757.

18 K. Landfester, *Adv. Mater.*, 2001, **13**, 765–768.
19 J. K. Oh, S. A. Bencherif and K. Matyjaszewski, *Polymer*, 2009, **50**, 4407–4423.
20 K. Raghupathi, S. J. Eron, F. Anson, J. A. Hardy and S. Thayumanavan, *Mol. Pharm.*, 2017, **14**, 4515.
21 S. M. Standley, Y. J. Kwon, N. Murthy, J. Kunisawa, N. Shastri, S. J. Guillaudeu, L. Lau and J. M. J. Fréchet, *Bioconjugate Chem.*, 2004, **15**, 1281–1288.
22 N. Murthy, M. Xu, S. Schuck, J. Kunisawa, N. Shastri and J. M. J. Fréchet, *Proc. Natl. Acad. Sci. U. S. A.*, 2003, **100**, 4995.
23 M. A. Azagarsamy, D. L. Alge, S. J. Radhakrishnan, M. W. Tibbitt and K. S. Anseth, *Biomacromolecules*, 2012, **13**, 2219.
24 J. X. Zhong, J. R. Clegg, E. W. Ander and N. A. Peppas, *J. Biomed. Mater. Res., Part A*, 2018, **106**, 1677–1686.